



Deep learning radiomics model based on PET/CT predicts PD-L1 expression in non-small cell lung cancer

Bo Li¹, Jie Su¹, Kai Liu, Chunfeng Hu^{*}

Department of Radiology, Affiliated Hospital of Xuzhou Medical University, Xuzhou Medical University, Xuzhou, China

ARTICLE INFO

Keywords:
 Radiomics
 Deep learning
 Machine learning
 PD-L1
 PET/CT
 Non-small cell lung cancer

ABSTRACT

Purpose: Programmed cell death protein-1 ligand (PD-L1) is an important prognostic predictor for immunotherapy of non-small cell lung cancer (NSCLC). This study aimed to develop a non-invasive deep learning and radiomics model based on positron emission tomography and computed tomography (PET/CT) to predict PD-L1 expression in NSCLC.

Methods: A total of 136 patients with NSCLC between January 2021 and September 2022 were enrolled in this study. The patients were randomly divided into the training dataset and the validation dataset in a ratio of 7:3. Radiomics feature and deep learning feature were extracted from their PET/CT images. The Mann-whitney U-test, Least Absolute Shrinkage and Selection Operator algorithm and Spearman correlation analysis were used to select the top significant features. Then we developed a radiomics model, a deep learning model, and a fusion model based on the selected features. The performance of three models were compared by the area under the curve (AUC), sensitivity, specificity, accuracy, positive predictive value, and negative predictive value.

Results: Of the patients, 42 patients were PD-L1 negative and 94 patients were PD-L1 positive. A total of 2446 radiomics features and 4096 deep learning features were extracted per patient. In the training dataset, the fusion model achieved a highest AUC (0.954, 95% confident interval [CI]: 0.890–0.986) compared with the radiomics model (0.829, 95%CI: 0.738–0.898) and the deep learning model (0.935, 95%CI: 0.865–0.975). In the validation dataset, the AUC of the fusion model (0.910, 95% CI: 0.779–0.977) was also higher than that of the radiomics model (0.785, 95% CI: 0.628–0.897) and the deep learning model (0.867, 95% CI: 0.724–0.952).

Conclusion: The PET/CT-based deep learning radiomics model can predict the PD-L1 expression accurately in NSCLC patients, and provides a non-invasive tool for clinicians to select positive PD-L1 patients.

1. Introduction

Lung cancer is one of the most prevalent cancers, and accounts for 11.6% of cancer incidence and 18.4% of cancer-related mortality worldwide [1]. Non-small cell lung cancer (NSCLC) is the most common type of lung cancer, accounting for approximately 85% of all primary lung cancer cases [2]. In recent years, immune checkpoint inhibitors (ICIs) have emerged as a clinical hotspot and dramatically changed the treatment landscape of NSCLC [3]. ICI-based immunotherapy has shown remarkable success in improving survival outcomes of NSCLC. Programmed cell death protein-1 (PD-1) and programmed cell death protein-1 ligand (PD-L1), have been extensively used as predictive biomarkers for ICI-based immunotherapy in clinical trials [4,5]. Among the

various PD-L1 scoring methods, the tumor proportion score (TPS) is the most widely used in clinical practice [6]. The expression of PD-L1 is associated with the prognosis of patients with NSCLC, and studies have shown that patients with negative PD-L1 expression (TPS <1%) are not suitable for the treatment with anti-PD-L1 antibody, while patients with positive PD-L1 expression (TPS ≥1%) can benefit from anti-PD-L1 antibody [7,8]. However, traditional methods of PD-L1 detection, such as biopsy specimens or surgically resected tissue, are invasive and cannot reflect the dynamic changes in PD-L1 expression of NSCLC non-invasively [9]. Hence, there is an urgent need for a non-invasive tool that can dynamically assess PD-L1 expression and select suitable NSCLC patients for ICI-based immunotherapy in clinical practice. Such a tool would be extremely valuable in guiding the selection of appropriate

* Correspondence to: Department of Radiology, Affiliated Hospital of Xuzhou Medical University, Xuzhou Medical University, Xuzhou 221006, China.

E-mail address: hcfxz@163.com (C. Hu).

¹ These authors contributed equally to the manuscript

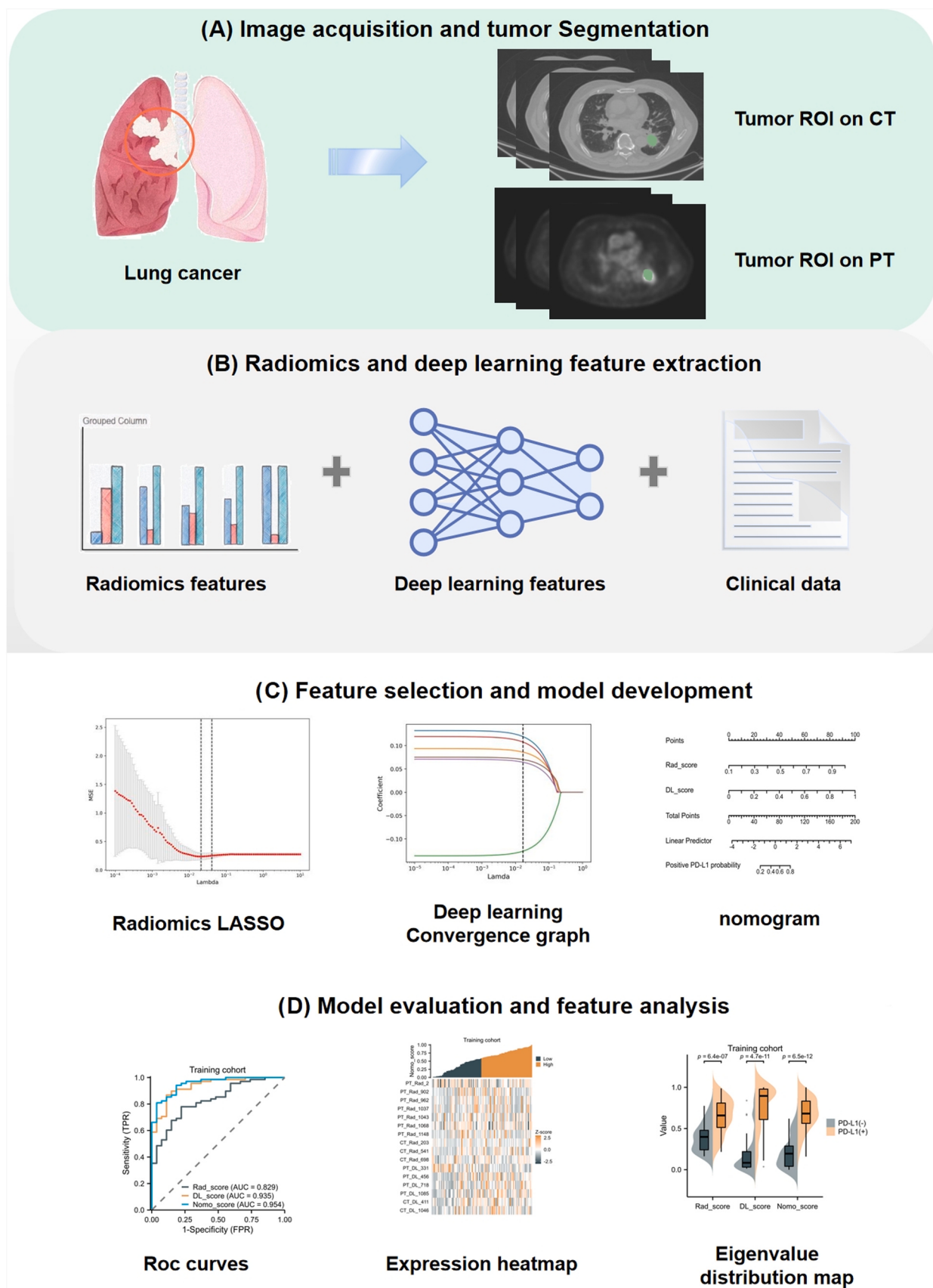


Fig. 1. Flowchart of this study.

Table 1

Comparison of basic clinical features of patients with PD-L1 negative expression and positive expression.

Characteristics	PD-L1 (-) (n = 42)	PD-L1 (+) (n = 94)	P value
Age	65.71 ± 7.03	63 ± 11.33	0.091
Diameter (mm), median (IQR)	31 (25.25, 41.75)	32 (22.25, 43.75)	0.687
Sex, n (%)			0.003
female	20 (14.7%)	21 (15.4%)	
male	22 (16.2%)	73 (53.7%)	
Smoking history, n (%)			0.013
no	33 (24.3%)	53 (39%)	
yes	9 (6.6%)	41 (30.1%)	
T stage, n (%)			0.773
1	18 (13.2%)	41 (30.1%)	
2	16 (11.8%)	39 (28.7%)	
3	5 (3.7%)	11 (8.1%)	
4	3 (2.2%)	3 (2.2%)	
N stage, n (%)			0.717
0	20 (14.7%)	37 (27.2%)	
1	2 (1.5%)	8 (5.9%)	
2	15 (11%)	34 (25%)	
3	5 (3.7%)	15 (11%)	
Clinical stage, n (%)			0.871
I	17 (12.5%)	32 (23.5%)	
II	4 (2.9%)	10 (7.4%)	
III	13 (9.6%)	35 (25.7%)	
IV	8 (5.9%)	17 (12.5%)	
Histological type, n (%)			0.155
SCC	10 (7.4%)	34 (25%)	
AC	32 (23.5%)	60 (44.1%)	
SUVmax, median (IQR)	11.35 (4.97, 15.67)	14 (9.42, 19.95)	0.024

treatment options for NSCLC patients and improving their survival outcome.

Radiomics is an emerging field that extracting and analyzing a lot of quantitative features from medical images, and it has the potential to predict cancer type, treatment response and prognosis [10]. It can be used to develop diagnostic and prognostic models for a variety of medical conditions, especially in cancer field [11,12]. The application of radiomics on PET/CT images has shown promising value in predicting various aspects of cancer, including tumor metabolism, tumor hypoxia, and even prognosis [13]. PET/CT examinations are widely used for NSCLC, as it can obtain more information of tumor metabolism and occult lesion detection [14]. Certain radiomics features were reported associating with genetic mutations and immunohistochemistry in NSCLC, and even have prognostic value in predicting progression-free survival or overall survival. Previous study has revealed that CT-derived radiomics model can non-invasively predict PD-L1 expression of NSCLC [15]. Deep learning techniques can also learn complex features from PET/CT images, and have shown superior performance in various image classification tasks [16]. Compared with artificially defined radiomics features, deep learning features are extracted by convolutional neural networks (CNNs) and contain more abstract medical image information [17]. However, no literature reports the combination of deep learning and radiomics for predicting PD-L1 expression of NSCLC on PET/CT images. Fusing valuable radiomics and deep learning features may accurately predict PD-L1 expression in NSCLC.

In this study, we recruited patients with NSCLC who had undergone preoperative PET/CT examination. We employed radiomics and deep learning methods to comprehensively extract relevant features from the patients' PET/CT, and utilized these features to develop different predictive models for predicting the PD-L1 expression of NSCLC accurately.

2. Materials and methods

2.1. Patient selection

This study enrolled a total of 136 patients with NSCLC from January 2021 to September 2022. Of the patients, 42 were PD-L1 negative and 94 were PD-L1 positive. The inclusion criteria were as follows: [1] pathologically confirmed NSCLC at initial diagnosis; [2] the PD-L1 status was determined by IHC; [3] patients underwent PET/CT imaging before treatment; [4] complete baseline data(sex, smoking history, T stage, N stage, clinical stage, histological type,

age, diameter, SUVmax). The exclusion criteria were as follows: [1] patients with a history of previous malignancy or current concomitant malignancy; [2] patients who received chemotherapy, radiation therapy, or surgical resection prior to PET/CT scan; [3] poor quality of PET/CT images or lack of PET or CT sequence. This study was approved by Medical Ethics Committee of the relevant hospital, with the approval number: XYFY2023-KL319-01. The study's workflow is showed in Fig. 1.

2.2. Immunohistochemical detection of PD-L1 expression

PD-L1 detection was performed on surgically resected tissue specimens using the IHC method. After the surgical excision, the specimens were fixed with 10% formaldehyde and embedded in paraffin. Subsequently, the specimens were sectioned, antigen-repaired, and blocked, followed by the dropwise addition of PD-L1 antibody (22C3 antibody, Dako, USA). The PD-L1 expression level was determined based on the tumor proportion score (TPS), which represents the percentage of partially or completely membrane-stained tumor cells at any intensity. The PD-L1 expression of NSCLC was classified into either negative (<1% or absence of reactivity) or positive ($\geq 1\%$) according to the TPS result [18].

2.3. PET/CT image acquisition and reconstruction

All patients underwent FDG-PET/CT examinations prior to surgery using the Discovery PET/CT Elite scanner (GE USA), which obtain CT images by the Light Speed 128-slice spiral CT machine. The imaging agent was 18 F-FDG, with a radiochemical purity of $> 95\%$. Before the PET/CT examination, patients were asked to avoid strenuous exercise for 24 h and fast for more than 6 h from food and drink. After obtaining the patient's height, weight, and blood sugar, the imaging agent was injected intravenously through the back of the hand or the elbow at a dose of 3.5–4.0 MBq/kg, while the fasting blood glucose was controlled below 150 g/L. After injection, patients rested quietly for 1 h and drank 600 ml of water. Patients were then asked to urinate before scanning and drank about 600 ml of water again. After adjusting the localization, CT scanning was performed from the top of the skull to the mid-thigh per patient. The scanning parameters were as follows: 120kV, 180 mA, rotation time 0.5 S/rev, pitch 1.375, thickness 3.75 mm, and layer spacing 3.25 mm. A total of 8 bed positions were collected for PET, with a collection time of 3 min per bed position. Finally, the CT data were used for attenuation correction, and iterative reconstruction was performed to obtain the whole-body CT, whole-body PET, and PET/CT fusion images.

2.4. Tumor radiation feature segmentation and extraction

In this study, the region of interest (ROI) was delineated by a nuclear medicine physician using 3D Slicer 4.10.1 software on each axial slice of CT and PET images. All ROIs were reviewed by two senior nuclear medicine physicians with more than 10 years' experience, and a third senior nuclear medicine physician with more than 15 years' experience made the final decision to ROI when disagreements occurred between two physicians. The actual boundary of PET was determined by

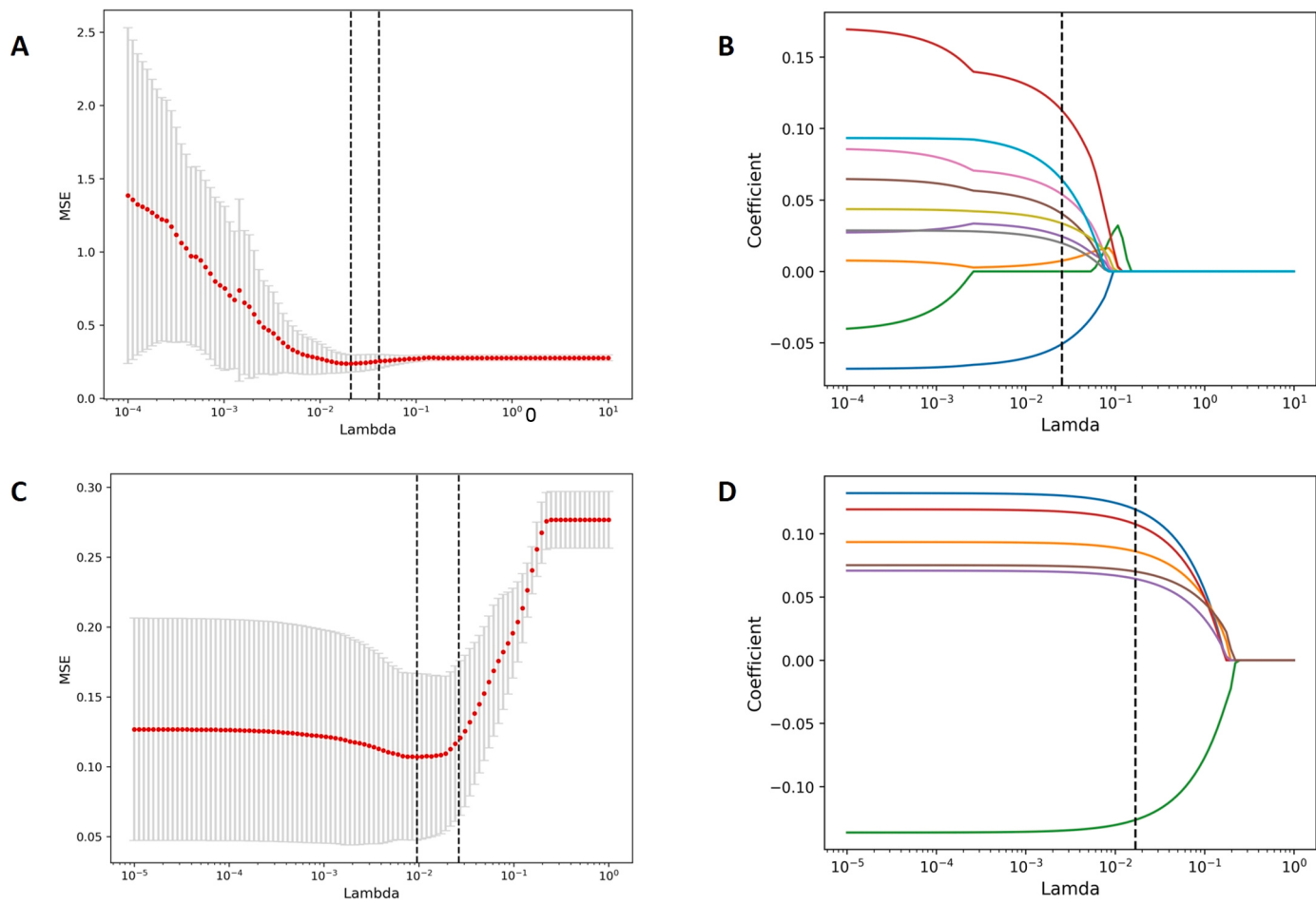


Fig. 2. The optimal features were selected by the LASSO algorithm to construct the final radiology model (A) and deep learning model (C). Lasso coefficients (B,D) for preserved radiological features and deep learning features.

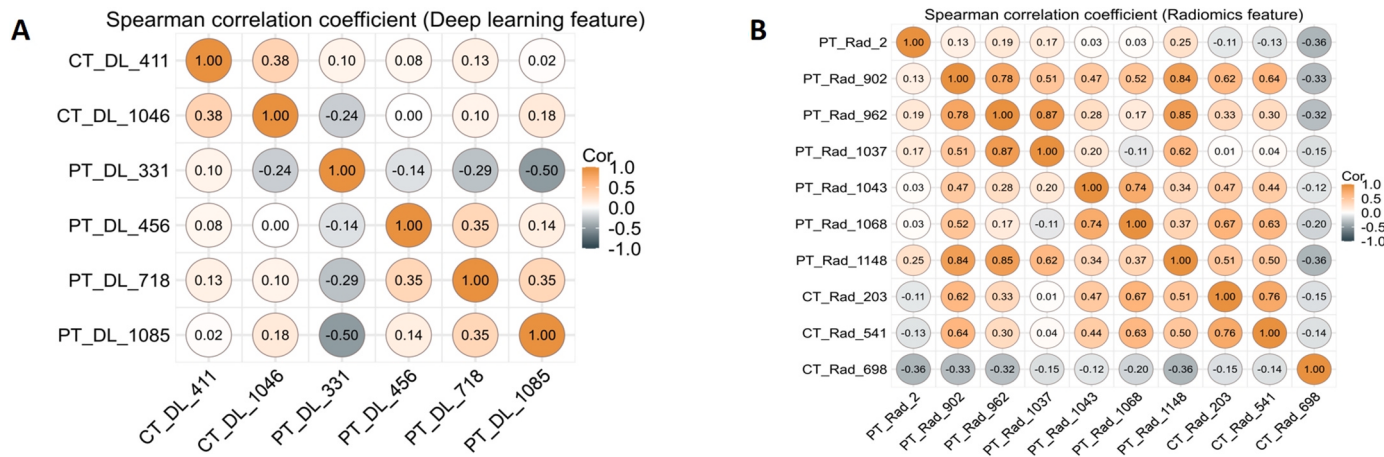


Fig. 3. (A) and (B) showed the Spearman rank correlation coefficient between the radiological and deep learning features, respectively.

reference the PET iamges to the CT images.

After ROI delianation, the original CT and PET images and their corresponding ROIs were input into the PyRadiomic module in 3D slicer to extract radiomics features. The radiomics features of the PET/CT images could be divided into seven classes: [1] shape-based feature, [2] first-order histogram features, [3] gray-level cooccurrence matrix (GLCM) features, [4] Gray-level run length matrix (GLRLM) features, [5] Gray-level size zone matrix (GLSZM) features, [6] Neighboring gray

tone difference matrix (NGTDM) features, and [7] Gray-level dependence matrix (GLDM) features. To obtain more image-derived features, high-dimensional image analysis was performed on CT and PET images using image filters including Wavelet and Gaussian filters. Finally, a total of 2446 features were extracted from the PET and CT images for further analysis per patient.

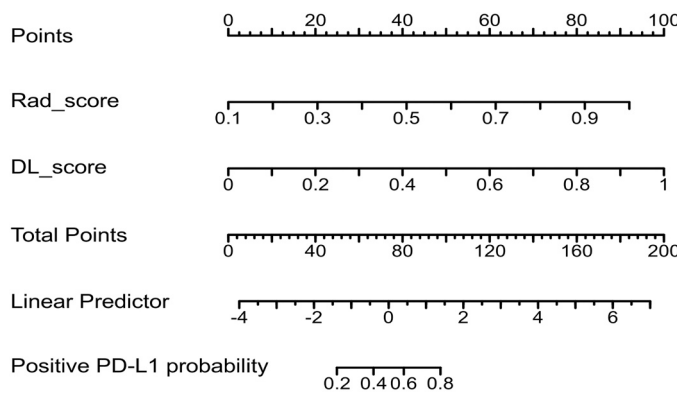


Fig. 4. A nomogram of the fusion model based on radiology scores and deep learning scores.

2.5. Deep learning feature extraction

In this study, a convolutional neural network (CNN) based on the ResNet-101 architecture was developed to extract deep learning features from the PET/CT images. An experienced radiologist visually selected the level that included the largest tumor area and cropped a rectangular bounding patch covering the entire tumor area and about 5 mm peritumor region. Then the patches of CT and PET sequences were resized to a two-dimensional matrix of 512×512 , as to adjust to the input of ResNet-101 model. All patches containing more than 75% of the tumor area were input into the ResNet-101 model. The model analyzed the images and extracting deep learning features from the fully connected layer. Finally, a total of 4096 features were obtained from PET and CT images per patient.

2.6. Feature selection and model establishment

The 136 patients were randomly split into two groups at a ratio of 7:3, resulting 95 patients for model training and 41 patients for model validation. The large number of imaging features may cause overfitting. Thus, feature dimension reduction was necessary to ensure the model's robustness. The machine learning model constructions were performed for radiomics feature and deep learning feature, respectively. Firstly, the Mann-Whitney U test was used to eliminate redundant radiomics features with p -values > 0.05 . Secondly, the LASSO algorithm identified the most significant non-zero coefficient features through repeated cross-validation. Thirdly, a linear logistic regression model was developed using selected radiomics features. The radiomics signature for each patient in the training cohort and validation cohort was calculated. For deep learning feature, by iterating above steps, a deep learning model was constructed, and the deep learning signature was calculated for each patient as well. Furthermore, logistic regression analysis was performed to integrate radiomics signature and deep learning signature and develop a nomogram which can calculate the total probability of positive PD-L1.

2.7. Statistical analysis

Various statistical methods were used to assess the group difference of clinical features in positive PD-L1 and negative PD-L1 NSCLC patients. Categorical variables (sex, smoking history, T stage, N stage, clinical stage, histological type) were analyzed using the chi-square test, while continuous variables (age, diameter, SUVmax) were statistical with the student's t test or Mann-Whitney U test. Two-sided p -values < 0.05 were deemed statistically significant. Spearman correlation analysis was used to evaluate the association between features. Moreover, model performance was assessed using the area under curve (AUC), accuracy, sensitivity, specificity, positive and negative predictive

values.

3. Result

3.1. Clinical characteristics

A total of 136 patients with NSCLC were included in this study, comprising 42 PD-L1-negative patients and 94 PD-L1-positive patients. The clinical characteristics of patients are presented in Table 1. Among the patients, statistically significant differences were observed in SUVmax ($p = 0.024$), sex ($p = 0.003$) and smoking history ($p = 0.013$) between the two cohorts. However, no significant differences were observed in other characteristics, including age, lesion diameter, clinical T stage, clinical N stage, and histological type.

3.2. Feature selection and model establishment

In this study, we extracted a total of 1223 radiomics features from PET images and 1223 radiomics features from CT images. A total of 1223 quantitative imaging features including four categories: 14 shape based features, 18 first order statistical features, 75 textural features from original images and 1116 transformation features. After the Mann-Whitney U test, 693 features were selected for further analysis. The LASSO algorithm was then used to select the most significant features. Out of the selected features, 7 features were derived from PET images and 3 features from CT images, including two categories: 1 shape based feature and 9 transformation features. The features were used to establish a radiomics model (Rad_model) by linear logistic regression. The radiomics score for each patient was then calculated by the Rad_model (see Fig. 2). In the DenseNet-101 model, the fully connected layer and softmax layer were removed, and the output value of the nodes in last layer was used as deep learning features. In this way, we extracted 2048 deep learning features from CT tumor-region images and 2048 deep learning features PET tumor-region images. Using the LASSO algorithm, we identified 6 features, with 4 extracted from PET images and 2 extracted from CT images. Similarly, a linear logistic regression model (DL_model) was developed to calculate the deep learning score for each patient in both the training and validation cohorts (Fig. 2).

We conducted Spearman correlation analysis for all radiomics and deep learning features, and no significant correlation was observed. The Spearman correlation coefficient between all features was consistently below 0.9, as showed in Fig. 3.

To improve the performance of model, a fusion model (Nomo_model) was developed by combining Rad_model and DL_model scores (Fig. 4). Utilizing personalized predictions for the training cohort, the nomogram provided a visual representation of the prediction results. This facilitated a more accurate assessment of the PD-L1 expression based on multi-factors data.

3.3. Performance evaluation

The ROC curves of three models (Rad_model, DL_model, Nomo_model) were presented in Fig. 5 A and 5B for both the training and validation cohorts. In the training cohort, the Rad_model achieved an AUC of 0.829 (95% CI: 0.738–0.898), the DL_model achieved an AUC of 0.935 (95% CI: 0.865–0.975), and the Nomo_model achieved the highest AUC of 0.954 (95% CI: 0.890–0.986). Similarly, in the validation cohort, the AUC scores were 0.785 (95% CI: 0.628–0.897), 0.867 (95% CI: 0.724–0.952), and 0.910 (95% CI: 0.779–0.977) for the Rad_model, DL_model, and Nomo_model, respectively. Notably, the Nomo_model outperformed the other two models in both the training and validation cohorts, as AUC showed.

The performance of the three models in both cohorts is summarized in Table 2. The Nomo_model exhibited sensitivities of 80.88% and 76.92% in the training and validation cohorts, respectively. The specificities were the highest, with values of 96.30% and 100%, respectively.

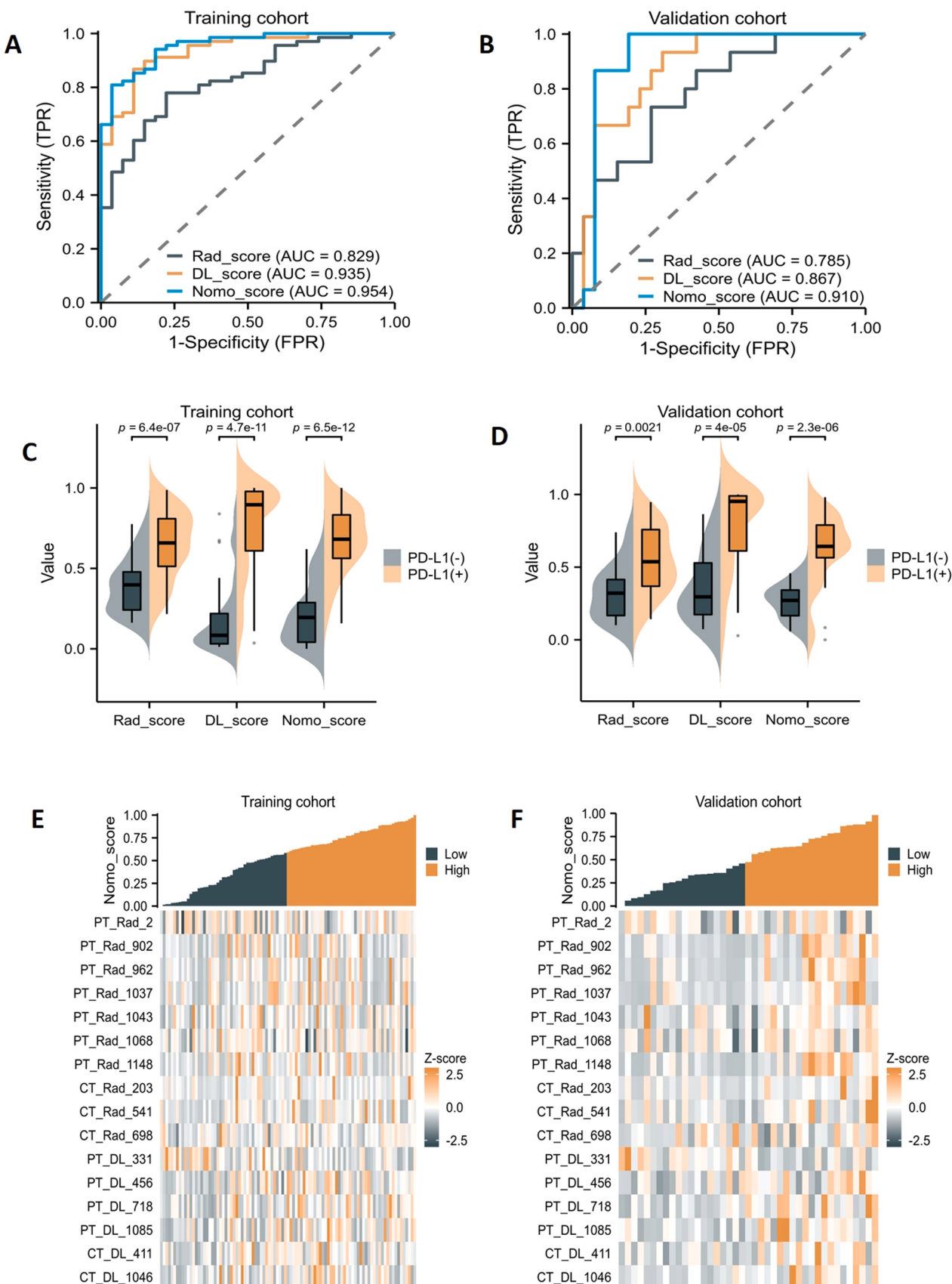


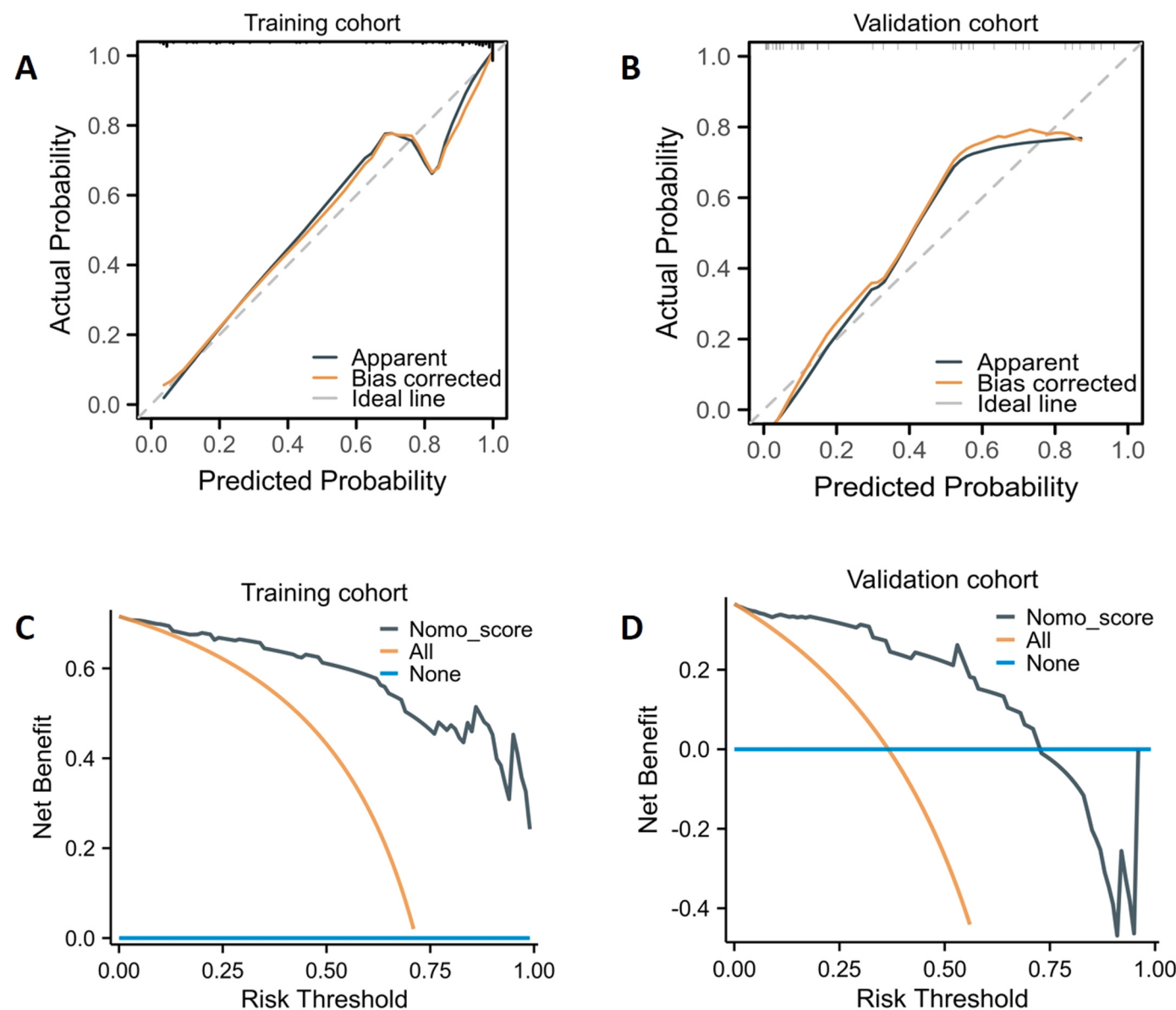
Fig. 5. (A) and (B) showed the ROC curves of three models (Rad, DL, Nomo) predicting the expression state of PD-L1 in the training and validation cohorts.(C) and (D) showed the distribution of feature values box plots for three models in the PD-L1-positive group and PD-L1-negative group in two cohorts.(E) and (F) showed a heat map of the expression of nemo scores in both cohorts for the PD-L1-positive group and the PD-L1-negative group.

Table 2

Diagnostic performance of the three models in training and validation cohorts.

	Rad_score training	Rad_score validation	DL_score training	DL_score validation	Nomo_score training	Nomo_score validation
AUC(95%CI)	0.829(0.738-0.898)	0.785(0.628-0.897)	0.935(0.865-0.975)	0.867(0.724-0.952)	0.954(0.890-0.986)	0.910(0.779-0.977)
ACC	77.89	65.85	87.37	75.61	85.26	85.37
SEN	77.94	57.69	86.76	80.77	80.88	76.92
SPE	77.78	80	88.89	66.67	96.30	100
PPV	89.83	83.33	95.16	80.77	98.21	100
NPV	58.33	52.17	72.73	66.67	66.67	71.43
cutoff	0.47918	0.47918	0.44044	0.44044	1.75746	1.75746

AUC, the area under the curve; ACC, accuracy; SEN, sensitivity; SPE, specificity; PPV, positive predictive value; NPV, negative predictive value; CUTOFF, cut off value.

**Fig. 6.** The calibration curves of the training and validation cohorts(A and B).The decision curves analysis in training and validation cohorts(C and D).

The accuracies of the Nomo_model were 85.26% and 85.37% in the training and validation cohorts, respectively. In Fig. 5 C and 5D, the distribution of feature values is depicted for three models in both cohorts. Notably, higher Nomo_model scores in PD-L1-positive patients were observed, with scores close to 1. Conversely, the lower Nomo_model scores were associated with PD-L1-negative patients, with scores closer to 0. Figs. 5E and 5 F presented a heat map illustrating the

expression of Nomo_model scores in both cohorts.

Figs. 6A and 6B displayed the calibration curves for the training and validation cohorts, demonstrating the favorable agreement between the predicted results and the true results. Using the fusion model to determine the PD-L1 status, patients can potentially benefit further. The decision curves analysis was conducted in both the training and validation cohorts, as shown in Figs. 6C and 6D.

4. Discussion

This study highlights the significance of radiomics and deep learning for predicting the expression of PD-L1 in NSCLC. The fusion model outperformed both the radiomics and deep learning models, demonstrating higher AUC and accuracy, thus exhibiting improved efficiency. In the training and validation cohorts, the fusion model achieved AUCs of 0.954 and 0.910, respectively. Moreover, the decision curve analysis illustrated greater clinical benefits, while the fusion model provided doctors with a non-invasive tool to determine the PD-L1 expression.

PD-L1 expression has been observed in various tumor cells, including NSCLC [19–22]. Cancer cells often develop special mechanisms to evade immune surveillance, resulting in metastasis [23]. These mechanisms involve the activation of PD-1 receptors, which enable cancer cells to evade immune surveillance [24]. PD-L1 expression is considered an important predictive biological marker in clinical practice [25]. There is increasing clinical evidence supporting the effectiveness of PD1/PD-L1 inhibitors in lung cancer [26]. Many studies have demonstrated that PD-1 or PD-L1 inhibitors offer greater benefits, prolonged overall survival, and improved tolerability in PD-L1-positive patients [27–31].

Immunohistochemistry (IHC) is currently used for assessing PD-L1 expression [32]. Some studies have demonstrated the potential of radiomics using PET/CT images for non-invasive detection of PD-L1 status [33,34]. However, deep learning radiomics offers several advantages over traditional methods for assessing PD-L1 expression. Firstly, deep learning radiomics predicts PD-L1 expression based on radiomics and deep learning features, eliminating the need for additional laboratory testing procedures and reducing the time required for operation. Secondly, it is a non-invasive approach that avoids patient discomfort during surgery, unlike IHC, which requires obtaining tumor tissue through biopsy or other invasive procedures. Thirdly, IHC interpretation relies on pathologists, making the results susceptible to external factors such as interpreter ability. In contrast, deep learning radiomics is achieved through automated algorithms with minimal interference. Therefore, evaluating PD-L1 expression through deep learning radiomics model holds significant value.

Radiomics and deep learning techniques have been widely explored to extract quantitative features from medical images, particularly in NSCLC. However, the application of a fusion model based on PET/CT deep learning radiomics for predicting PD-L1 expression in NSCLC is limited. Previous studies have demonstrated that when PD-L1 expression > 1% and > 50%, the corresponding AUCs of radiological predictions were 0.754 and 0.762, respectively. Combining clinical information with radiomics features improved the predictive performance, with AUC values of 0.762 and 0.814 for PD-L1 expression of > 1% and > 50%, respectively [35]. Non-invasive models that effectively predict EGFR mutation and PD-L1 expression are crucial for determining the therapy strategy for NSCLC patients [36]. Deep learning models have proven to be a non-invasive approach for accurately predicting high PD-L1 expression in NSCLC compared to immunohistochemistry [37]. A study revealed that deep learning models based on PET/CT images outperformed radiomics models in diagnosing EGFR mutation status in NSCLC. The deep learning model achieved a higher AUC value (0.90, 95% CI: 0.85–0.95) in the training set of 138 patients, compared to the radiology model (AUC: 0.82, 95% CI: 0.75–0.89) [38]. Wei et al. successfully developed deep learning scores to predict PD-L1 expression status, which has high prognostic value for predicting durable clinical benefit (DCB), progression-free survival (PFS), and overall survival (OS) in immunotherapy of NSCLC patients [39]. Similarly, in our study, the radiomics model (Rad_model) and deep learning model (DL_model) achieved AUCs of 0.829 (95% CI: 0.738–0.898) and 0.935 (95% CI: 0.865–0.975), respectively, with slightly superior performance observed in the deep learning model (DL) for predicting PD-L1 expression.

This study has some limitations as well. Firstly, due to the retrospective nature of this study, certain relevant clinical characteristics

were not included or were unavailable. Including comprehensive clinical information in future studies can improve the performance of the model. Secondly, the manual delineation of ROI and image segmentation methods used in this study had limitations in terms of repeatability, time consumption, labor intensity, and the expertise required by the operator. Future research should focus on developing reliable and accurate automated segmentation methods. Thirdly, the patient size was relatively small, and the study was conducted in a single institution. Large-sample, multi-center studies are warranted in the future to validate the models.

5. Conclusions

This study demonstrates that PET/CT-based deep learning radiomics model can accurately predict PD-L1 expression in NSCLC. The fusion model might offer a novel and non-invasive tool for clinicians to identify PD-L1-positive patients.

CRediT authorship contribution statement

Su Jie: Writing – original draft, Methodology, Data curation, Conceptualization. **Li Bo:** Writing – original draft, Methodology, Data curation, Conceptualization. **Hu Chunfeng:** Writing – review & editing, Methodology. **Liu Kai:** Writing – review & editing, Methodology, Funding acquisition, Data curation, Conceptualization.

Declaration of Competing Interest

The authors declare that they have no known competing financial interests or personal relationships that could have appeared to influence the work reported in this paper.

Appendix A. Supporting information

Supplementary data associated with this article can be found in the online version at doi:10.1016/j.ejro.2024.100549.

References

- [1] H. Sung, J. Ferlay, R.L. Siegel, et al., Global Cancer Statistics 2020: GLOBOCAN Estimates of Incidence and Mortality Worldwide for 36 Cancers in 185 Countries, CA Cancer J. Clin. 71 (3) (2021) 209–249.
- [2] J.R. Brahmer, R. Govindan, R.A. Anders, et al., The Society for Immunotherapy of Cancer consensus statement on immunotherapy for the treatment of non-small cell lung cancer (NSCLC), J. Immunother. Cancer 6 (1) (2018) 75.
- [3] A. Rittmeyer, F. Barlesi, D. Waterkamp, et al., Atezolizumab versus docetaxel in patients with previously treated non-small-cell lung cancer (OAK): a phase 3, open-label, multicentre randomised controlled trial, Lancet 389 (10066) (2017) 255–265.
- [4] A. Tunger, M. Kießler, R. Wehner, et al., Immune monitoring of cancer patients prior to and during CTLA-4 or PD-1/PD-L1 inhibitor treatment, Biomedicines 6 (1) (2018) 26.
- [5] D.S. Chen, B.A. Irving, F.S. Hodi, Molecular pathways: next-generation immunotherapy-inhibiting programmed death-ligand 1 and programmed death-1, Clin. Cancer Res 18 (24) (2012) 6580–6587.
- [6] H. Rizvi, F. Sanchez-Vega, K. La, et al., Molecular determinants of response to anti-programmed cell death (PD)-1 and anti-programmed death-ligand 1 (PD-L1) blockade in patients with non-small-cell lung cancer profiled with targeted next-generation sequencing, J. Clin. Oncol. 36 (7) (2018) 633–641.
- [7] D.B. Doroshow, S. Bhalla, M.B. Beasley, et al., PD-L1 as a biomarker of response to immune-checkpoint inhibitors, Nat. Rev. Clin. Oncol. 18 (6) (2021) 345–362.
- [8] T.S.K. Mok, Y.L. Wu, I. Kudaba, et al., Pembrolizumab versus chemotherapy for previously untreated, PD-L1-expressing, locally advanced or metastatic non-small-cell lung cancer (KEYNOTE-042): a randomised, open-label, controlled, phase 3 trial, Lancet 393 (10183) (2019) 1819–1830.
- [9] J. McLaughlin, G. Han, K.A. Schalper, et al., Quantitative Assessment of the Heterogeneity of PD-L1 Expression in Non-Small-Cell Lung Cancer [published correction appears in JAMA Oncol. 2016 Jan;2(1):146], JAMA Oncol. 2 (1) (2016) 46–54.
- [10] E.P. Huang, J.P.B. O'Connor, L.M. McShane, et al., Criteria for the translation of radiomics into clinically useful tests, Nat. Rev. Clin. Oncol. 20 (2) (2023) 69–82.
- [11] M.E. Mayerhofer, A. Materka, G. Langs, et al., Introduction to radiomics, J. Nucl. Med. 61 (4) (2020) 488–495.

- [12] R.J. Gillies, P.E. Kinahan, H. Hricak, Radiomics: images are more than pictures, they are data, *Radiology* 278 (2) (2016) 563–577.
- [13] B. Xue, J. Jiang, L. Chen, S. Wu, et al., Development and validation of a radiomics model based on 18F-FDG PET of primary gastric cancer for predicting peritoneal metastasis, *Front. Oncol.* 11 (2021) 740111.
- [14] A.T. Mayer, S.S. Gambhir, The immunoiimaging toolbox, *J. Nucl. Med.* 59 (8) (2018) 1174–1182.
- [15] M. Jiang, D. Sun, Y. Guo, et al., Assessing PD-L1 expression level by radiomic features from PET/CT in nonsmall cell lung cancer patients: an initial result, *Acad. Radio.* 27 (2) (2020) 171–179.
- [16] W. Mu, L. Jiang, Y. Shi, I. Tunali, J.E. Gray, et al., Non-invasive measurement of PD-L1 status and prediction of immunotherapy response using deep learning of PET/CT images, *J. Immunother. Cancer* 9 (6) (2021) e002118.
- [17] X. Li, L. Yang, X. Jiao, Comparison of traditional radiomics, deep learning radiomics and fusion methods for axillary lymph node metastasis prediction in breast cancer, *Acad. Radio.* 30 (7) (2023) 1281–1287.
- [18] H. Yu, T.A. Boyle, C. Zhou, et al., PD-L1 expression in lung cancer [published correction appears in *J Thorac Oncol.* 2017 Jan;12 (1):157–159], *J. Thorac. Oncol.* 11 (7) (2016) 964–975.
- [19] F.K. Dermani, P. Samadi, G. Rahmani, et al., PD-1/PD-L1 immune checkpoint: potential target for cancer therapy, *J. Cell Physiol.* 234 (2) (2019) 1313–1325.
- [20] Y. Masugi, R. Nishihara, J. Yang, et al., Tumour CD274 (PD-L1) expression and T cells in colorectal cancer, *Gut* 66 (8) (2017) 1463–1473.
- [21] E.A. Mittendorf, A.V. Phillips, F. Meric-Bernstam, et al., PD-L1 expression in triple-negative breast cancer, *Cancer Immunol. Res.* 2 (4) (2014) 361–370.
- [22] L. Gu, M. Chen, D. Guo, et al., PD-L1 and gastric cancer prognosis: a systematic review and meta-analysis, *PLoS One* 12 (8) (2017) e0182692.
- [23] Y. Liu, X. Cao, Immunosuppressive cells in tumor immune escape and metastasis, *J. Mol. Med. (Berl.)* 94 (5) (2016) 509–522.
- [24] X. Wang, F. Teng, L. Kong, et al., PD-L1 expression in human cancers and its association with clinical outcomes, *Onco Targets Ther.* 9 (2016) 5023–5039.
- [25] G.T. Gibney, L.M. Weiner, M.B. Atkins, Predictive biomarkers for checkpoint inhibitor-based immunotherapy, *Lancet Oncol.* 17 (12) (2016) e542–e551.
- [26] J.X. Li, J.M. Huang, Z.B. Jiang, et al., Current clinical progress of PD-1/PD-L1 immunotherapy and potential combination treatment in non-small cell lung cancer, *Integr. Cancer Ther.* 18 (2019), 1534735419890020.
- [27] L. Horn, D.R. Spigel, E.E. Vokes, et al., Nivolumab versus docetaxel in previously treated patients with advanced non-small-cell lung cancer: two-year outcomes from two randomized, open-label, phase III Trials (CheckMate 017 and CheckMate 057), *J. Clin. Oncol.* 35 (35) (2017) 3924–3933.
- [28] J. Brahmer, K.L. Reckamp, P. Baas, et al., Nivolumab versus docetaxel in advanced squamous-cell non-small-cell lung cancer, *N. Engl. J. Med.* 373 (2) (2015) 123–135.
- [29] R.J. Motzer, B. Escudier, D.F. McDermott, et al., Nivolumab versus everolimus in advanced renal-cell carcinoma, *N. Engl. J. Med.* 373 (19) (2015) 1803–1813.
- [30] H. Borghaei, L. Paz-Ares, L. Horn, et al., Nivolumab versus docetaxel in advanced nonsquamous non-small-cell lung cancer, *N. Engl. J. Med.* 373 (17) (2015) 1627–1639.
- [31] R.L. Ferris, G. Blumenschein Jr, J. Fayette, et al., Nivolumab for recurrent squamous-cell carcinoma of the head and neck, *N. Engl. J. Med.* 375 (19) (2016) 1856–1867.
- [32] L. Fehrenbacher, A. Spira, M. Ballinger, et al., Atezolizumab versus docetaxel for patients with previously treated non-small-cell lung cancer (POPLAR): a multicentre, open-label, phase 2 randomised controlled trial, *Lancet* 387 (10030) (2016) 1837–1846.
- [33] X. Wu, Y. Huang, Q. Zhao, et al., PD-L1 expression correlation with metabolic parameters of FDG PET/CT and clinicopathological characteristics in non-small cell lung cancer, *EJNMMI Res.* 10 (1) (2020) 51.
- [34] Y. Cui, X. Li, B. Du, et al., PD-L1 in Lung Adenocarcinoma: Insights into the Role of 18F-FDG PET/CT, *Cancer Manag. Res.* 12 (2020) 6385–6395.
- [35] J. Li, S. Ge, S. Sang, et al., Evaluation of PD-L1 expression level in patients with non-small cell lung cancer by 18F-FDG PET/CT radiomics and clinicopathological characteristics, *Front. Oncol.* 11 (2021) 789014.
- [36] C. Wang, X. Xu, J. Shao, et al., Deep learning to predict EGFR mutation and PD-L1 expression status in non-small-cell lung cancer on computed tomography images, *J. Oncol.* 2021 (2021) 5499385.
- [37] P. Tian, B. He, W. Mu, et al., Assessing PD-L1 expression in non-small cell lung cancer and predicting responses to immune checkpoint inhibitors using deep learning on computed tomography images, *Theranostics* 11 (5) (2021) 2098–2107.
- [38] W. Huang, J. Wang, H. Wang, et al., PET/CT based EGFR mutation status classification of NSCLC using deep learning features and radiomics features, *Front. Pharmacol.* 13 (2022) 898529.
- [39] W. Mu, L. Jiang, Y. Shi, et al., Non-invasive measurement of PD-L1 status and prediction of immunotherapy response using deep learning of PET/CT images, *J. Immunother. Cancer* 9 (6) (2021) e002118.